75th International Astronautical Congress (IAC), Milan, Italy, 14-18 October 2024.

IAC-24,C1,IP,14,x84302

On the refinement of low-energy Earth–Moon transfer families into an ephemeris model

Claudio Toquinho Campana[a*], **Francesco Topputo**[b]

[a,b] *Dept. of Aerospace Science and Technology, Politecnico di Milano, Via G. La Masa 34, 20156 Milano, Italy*
[*]Corresponding Author

Abstract

Interest in the exploitation of the cislunar environment is growing exponentially. The establishment of lunar outposts and orbiting gateways is pivotal to enable the next generation of human exploration in the solar system. This paper investigates the refinement process of prototype Earth–Moon transfers, originally designed in the Earth–Moon, Sun-perturbed bi-circular restricted four-body problem, into the full ephemeris. Reference bi-impulsive trajectories, extracted from a dataset of locally optimal solutions, serve as seeds for the generation of flyable cruises to the Moon in the real environment. Complex transfer geometries pose challenges in refinement. A meticulous search for a suitable departure calendar epoch is necessary to facilitate the process. Moreover, passage through an intermediate astrodynamic model, such as the elliptic one, further favors convergence to the high-fidelity representation. As a new era of lunar exploration approaches, this work demonstrates the flyability of complex Earth–Moon transfers within the real solar system, and elucidates the process of achieving such trajectories.
Keywords: Earth–Moon transfers, Cislunar environment, Ephemeris model, Trajectories refinement.

1 Introduction

Space exploration is witnessing a flourishing momentum, evidenced by the recent interest of private companies that, alongside national agencies, are laying the groundwork for the next space race era. Nowadays, the space domain and its exploitation are indeed considered strategical to the technological and scientific advancement of humanity. The colonization of our natural satellite is the first necessary step toward human expansion across regions of the solar system [1]. Many missions have been recently launched in the cislunar space (CAPSTONE [2], ArgoMoon [3], EQUULEUS [4], Chang'e-6) and many others are planned for the near future (e.g. LUMIO [5]). Current effort in advancing scientific and technological knowledge is laying the foundations for the incoming space era.

Among all challenges, the design of a spacecraft trajectory is a delicate process. Hence, the development of new analysis tools, methods, and procedures is paramount to enhance the efficiency and effectiveness of future space missions. As the dynamics governing the motion of a spacecraft becomes increasingly chaotic, the complexity of the problem grows exponentially [6]. The cislunar environment is an example of this. Here, the simultaneous presence of various attractive phenomena enables the design of unique trajectories. Traditional techniques, such as the patched conic approximation, though simple, fail to fully exploit the richness of the dynamics, thereby limiting their applicability. Conversely, overly complex models, albeit representing the real operative scenario, are impractical for generating space trajectories from scratch. Intermediate astrodynamic models are thus usually adopted to trade-off complexity and realism [7, 8].

Common trajectory design practices in the cislunar environment exploit natural dynamic structures of the Earth–Moon circular restricted three-body problem (CR3BP) [9, 10]. For example, invariant manifolds [6] emanating from periodic orbits [11] may enable efficient routes across the space. A more realistic framework is achieved by introducing the solar attraction in the model, thus obtaining the Earth–Moon, Sun-perturbed bi-circular restricted four-body problem (BCR4BP). Low-energy transfers crossing the outer region of the Earth–Moon realm can benefit this additional gravitational attraction to reduce the spacecraft fuel requirements [12, 13].

Recently, numerous studies addressed the problem of refining prototype trajectories into higher-fidelity models. A hierarchical structure of astrodynamic frameworks is adopted in [7] and [8] to smoothly transition into the ephemeris system through multiple shooting. A cooperative evolutionary algorithm is employed in [14] to optimize interior Earth–Moon transfers in the real system. [15–17] express transfer segments via the Theory of Functional Connections and a homotopy continuation approach is used for refinement purposes.

[a]Ph.D. Student, claudiotoquinho.campana@polimi.it
[b]Full Professor, francesco.topputo@polimi.it

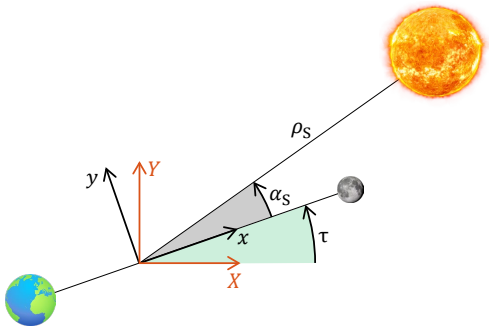

Fig. 1: BCR4BP model (not to scale). Non-rotating, quasi-inertial coordinates in orange.

In this work, several Earth–Moon bi-impulsive transfers of complex geometries, originally adhering to the BCR4BP dynamics, are transitioned into the real ephemeris. Suitable conditions enabling smooth refinements are investigated. The choice of the departure calendar epoch (ET_0) is critical. Therefore, a routine is proposed to set this important parameter. The benefit of passing through an intermediate astrodynamic model is assessed as well. The importance of this study lies in enhancing understanding of the dynamic rules governing lunar trajectories, thereby permitting more informed design practices for future missions.

The remainder of the paper is structured as follows. Section 2 introduces the dynamic models and describes the cislunar environment. In Sect. 3, the process of refining complex Earth–Moon transfers is idealized. The procedure is then practiced in Sect. 4 and eventually conclusions are drawn in Sect. 5.

2 Background

2.1 Dynamic models

2.1.1 Earth–Moon, Sun-perturbed bi-circular restricted four-body problem

In the BCR4BP, the Earth and the Moon revolve circularly about their common barycenter which, in turn, orbits the Sun as depicted in Fig. 1. The equations of motions are formulated in the rotating frame (rf) centered at the Earth–Moon barycenter, with the x axis directed toward the Moon. In the planar problem, the non-dimensional dynamics is expressed as [18]

$$\begin{aligned} \ddot{x} &= 2\dot{y} + \frac{\partial \Omega_4}{\partial x} \\ \ddot{y} &= -2\dot{x} + \frac{\partial \Omega_4}{\partial y}, \end{aligned} \tag{1}$$

Tab. 1: Normalized BCR4BP physical parameters.

Sym.	Value	Description
μ	$1.215\,066\,830\times10^{-2}$	Mass parameter
m_S	$3.289\,005\,410\times10^{5}$	Sun mass
ρ_S	$3.888\,111\,430\times10^{2}$	EM–S distance
ω_S	$-9.251\,959\,850\times10^{-1}$	Sun angular velocity

where

$$\begin{aligned} \Omega_4 = &\frac{1}{2}(x^2+y^2) + \frac{1-\mu}{r_E} + \frac{\mu}{r_M} + \frac{1}{2}\mu(1-\mu) + \\ &+ \frac{m_S}{r_S} - \frac{m_S}{\rho_S^2}\big(x\cos(\alpha_S) + y\sin(\alpha_S)\big) \end{aligned} \tag{2}$$

is the effective potential and

$$\alpha_S = \omega_S(\tau - \tau_0) + \alpha_S\big|_{\tau_0} \tag{3}$$

is the instantaneous Sun phase angle in the rotating frame. The quantity r_i represents the scaled distance of the spacecraft from the ith celestial body. In this frame, the Earth is fixed at $[-\mu, 0]$, whereas the Moon rests at $[1-\mu, 0]$. Table 1 reports the non-dimensional values adopted to generate the original prototype trajectories.

2.1.2 Earth–Moon, Sun-perturbed elliptic restricted problem

In the hierarchical ladder of astrodynamic models, an higher level of fidelity is achieved by adopting the Earth–Moon, Sun-perturbed elliptic restricted problem (ERP). This framework differs from the BCR4BP due to the introduction of the real Earth–Moon pulsation, thereby accounting for their relative orbital eccentricity e. The non-dimensional equations of motions, defined in a roto-pulsating frame (RPF), are [19]

$$\begin{aligned} x'' &= 2y' + \frac{\partial \omega_4}{\partial x} \\ y'' &= -2x' + \frac{\partial \omega_4}{\partial y}, \end{aligned} \tag{4}$$

where

$$\omega_4 = (1 + e\cos f)^{-1}\Omega_4 \tag{5}$$

is the new effective potential. The true anomaly f of the relative elliptic orbit of the primaries is the new independent variable, hence the adoption of primes to denote derivatives. The pulsation makes the system rotating in a non-uniform fashion, even though unitary mean motion and Earth–Moon distance are obtained after normalization. The orbital period of the primaries equals 2π, and

$$\frac{\partial f}{\partial \tau} = \frac{(1 + e\cos f)^2}{(1-e^2)^{3/2}} \tag{6}$$

relates the true anomaly to the non-dimensional time [7]. Furthermore, the non-dimensional time past initial pericenter, τ_{peri}, can be retrieved from standard equations for elliptic orbits,

$$\begin{aligned} E &= 2\tan^{-1}\left(\sqrt{\frac{1-e}{1+e}}\,\tan\frac{f}{2}\right) \\ \tau_{\text{peri}} &= E - e\sin E + 2k\pi, \end{aligned} \tag{7}$$

where E is the eccentric anomaly and k tracks the number of pericenter crossings.

The Sun is still assumed to revolve circularly about the Earth–Moon barycenter at a distance scaled by the instantaneous Earth–Moon separation. To compute the solar phase angle in the RPF, it is necessary to transition through the quasi-inertial frame whose X axis aligns with the eccentricity vector. The transfer elapsed time past departure can be computed using Eq. (7)

$$\Delta\tau = \tau_{\text{peri}}\big|_f - \tau_{\text{peri}}\big|_{f_0}. \tag{8}$$

Consequently, the Sun angle θ_{S} with respect to the quasi-inertial frame is derived similarly to Eq. (3) as

$$\theta_{\text{S}}\big|_f = f_0 + \alpha_{\text{S}}\big|_{f_0} + \omega_{\text{S}}^*\,\Delta\tau, \tag{9}$$

where the Sun inertial angular velocity is $\omega_{\text{S}}^* = \omega_{\text{S}} + 1$ due to the unitary mean motion. Finally, the Sun phase angle in the RPF is retrieved as

$$\alpha_{\text{S}}\big|_f = \theta_{\text{S}}\big|_f - f. \tag{10}$$

2.1.3 Roto-pulsating, restricted n-body problem

The ephemeris model most accurately describes the real dynamics experienced by a spacecraft. Under the hypothesis of restricted motion, the acceleration of a body with respect to an inertial reference frame at the solar system barycenter (SSB) is, in dimensional units,

$$\ddot{\boldsymbol{R}} = \sum_{j=\mathcal{B}} -\mu_j \frac{\boldsymbol{R}-\boldsymbol{R}_j}{\|\boldsymbol{R}-\boldsymbol{R}_j\|^3} + \boldsymbol{a}_{\text{pert}}, \tag{11}$$

where the first term represents the gravitational attraction of all celestial bodies of interest, that is, the Sun, the Moon, and the planets. Ephemeris data are retrieved from the JPL DE440 [20] file through the SPICE toolkit [21, 22]. The second contribution in Eq. (11) models additional perturbative phenomena, which in this study reduce to the only solar radiation pressure (SRP) computed as [23]

$$\boldsymbol{a}_{\text{SRP}} = \text{SP}_0 \frac{\boldsymbol{R}-\boldsymbol{R}_{\text{Sun}}}{\|\boldsymbol{R}-\boldsymbol{R}_{\text{Sun}}\|^3}, \quad \text{SP}_0 = (1+c_{\text{r}})\,\frac{A_{\text{sc}}}{m_{\text{sc}}}\,\frac{\Psi_0 d_0^2}{c}. \tag{12}$$

Tab. 2: Values for SRP computation.

Sym.	Value	Description	Units
c_{r}	0.08	reflectivity coeff.	-
$\frac{A_{\text{sc}}}{m_{\text{sc}}}$	0.01	S/C area to mass ratio	m^2/kg
Ψ_0	1371	ref. solar flux	W/m^2
d_0	1	ref. E–S distance	AU
c	2.998×10^8	light speed	m/s

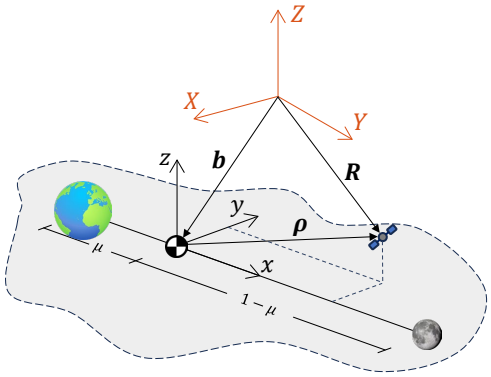

Fig. 2: RPF in black (not to scale). SSB frame in orange.

Refer to Table 2 for the numerical values adopted to estimate the SRP effect along the transfers.

To derive equations of motion resembling the formulation of the CR3BP, a high-fidelity RPF is introduced. In this system, the Earth and the Moon are at rest along the x axis, and are one non-dimensional unit apart. At any time instant, the RPF is constructed by retrieving the ephemeris states of the Earth and the Moon, thus computing the quantities [24]

$$\begin{aligned} \boldsymbol{b} &= \frac{M_{\text{E}}\boldsymbol{R}_{\text{E}} + M_{\text{M}}\boldsymbol{R}_{\text{M}}}{M_{\text{E}}+M_{\text{M}}} \\ k &= \|\boldsymbol{R}_{\text{E}} - \boldsymbol{R}_{\text{M}}\| \\ \boldsymbol{C} &= [\boldsymbol{e}_1, \boldsymbol{e}_2, \boldsymbol{e}_3], \end{aligned} \tag{13}$$

where

$$\begin{aligned} \boldsymbol{e}_1 &= \frac{\boldsymbol{R}_{\text{M}} - \boldsymbol{R}_{\text{E}}}{k} \qquad \boldsymbol{e}_2 = \boldsymbol{e}_3 \times \boldsymbol{e}_1 \\ \boldsymbol{e}_3 &= \frac{(\boldsymbol{V}_{\text{M}} - \boldsymbol{V}_{\text{E}}) \times (\boldsymbol{R}_{\text{M}} - \boldsymbol{R}_{\text{E}})}{\|(\boldsymbol{V}_{\text{M}} - \boldsymbol{V}_{\text{E}}) \times (\boldsymbol{R}_{\text{M}} - \boldsymbol{R}_{\text{E}})\|}. \end{aligned} \tag{14}$$

Consequently, as per Fig. 2, the relations

$$\begin{aligned} \boldsymbol{R} &= \boldsymbol{b} + k\boldsymbol{C}\boldsymbol{\rho} \\ \boldsymbol{V} &= \dot{\boldsymbol{b}} + \dot{k}\boldsymbol{C}\boldsymbol{\rho} + k\dot{\boldsymbol{C}}\boldsymbol{\rho} + k\boldsymbol{C}\boldsymbol{\rho}'\dot{\tau} \\ \tau &= n\,(\text{ET} - \text{ET}_0) \end{aligned} \tag{15}$$

permit to transform the state of a generic body from the SSB, i.e., $\{t, \boldsymbol{R}, \boldsymbol{V}\}$, to the RPF $\{\tau, \boldsymbol{\rho}, \boldsymbol{\rho}'\}$. In the RPF, the scaling factor $k(t)$ makes the Earth and the Moon occupy the same fixed positions they do in the CR3BP, thus accounting for their pulsation. A constant mean

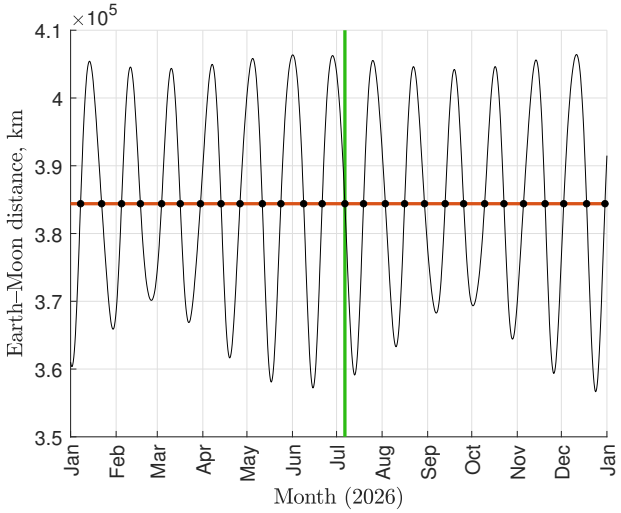

Fig. 3: Pulsation of primaries. Orange line indicates mean Earth–Moon distance (384 400 km). Green line relates to analysis in Sect. 3.2.

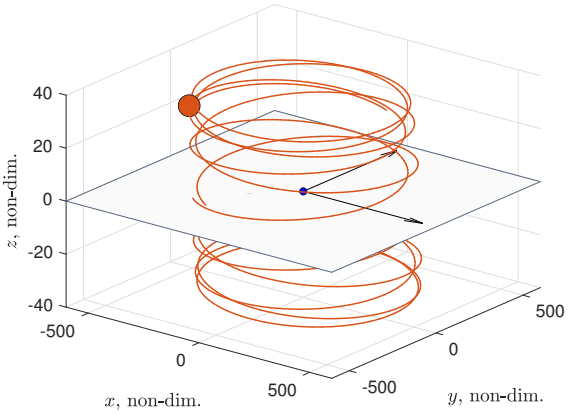

Fig. 4: Sun yearly revolution in Earth–Moon RPF. Not to scale for better visualization.

motion equal to

$$n = \frac{2\pi}{T} = \sqrt{\frac{\mathrm{G}(M_\mathrm{E} + M_\mathrm{M})}{\overline{d}^3}} \tag{16}$$

averages the primaries revolution period to 2π, with $\overline{d}$ representing their mean distance taken over a long time interval [7].

Finally, the spatial equations of motions for the rotopulsating, restricted n-body problem (RPRnBP) are derived by substituting Eq. (15) and its time derivative into Eq. (11), leading to

$$\begin{aligned}\boldsymbol{\rho}'' = &-\frac{1}{n^2}\left(\frac{\ddot{k}}{k}\boldsymbol{I} + \frac{2\dot{k}}{k}\boldsymbol{C}^\top\dot{\boldsymbol{C}} + \boldsymbol{C}^\top\ddot{\boldsymbol{C}}\right)\boldsymbol{\rho} + \\ &-\frac{2}{n}\left(\frac{\dot{k}}{k}\boldsymbol{I} + \boldsymbol{C}^\top\dot{\boldsymbol{C}}\right)\boldsymbol{\rho}' - \frac{\boldsymbol{C}^\top\ddot{\boldsymbol{b}}}{kn^2} + \\ &+\frac{1}{k^3n^2}\left(\sum_{j=\mathcal{B}} -\mu_j\frac{\boldsymbol{\delta}_j}{\|\boldsymbol{\delta}_j\|^3} + \mathrm{SP}_0\frac{\boldsymbol{\delta}_\mathrm{Sun}}{\|\boldsymbol{\delta}_\mathrm{Sun}\|^3}\right),\end{aligned} \tag{17}$$

where $\boldsymbol{\delta}_j = \boldsymbol{\rho} - \boldsymbol{\rho}_j$ and $\boldsymbol{\delta}_\mathrm{Sun} = \boldsymbol{\rho} - \boldsymbol{\rho}_\mathrm{Sun}$.

2.2 The cislunar environment

As mentioned in [18], the BCR4BP is deemed appropriate for capturing the basic behaviors characterizing the Sun–Earth–Moon system. However, the pulsation of the primaries, the non-coplanar motion of the Sun, and the presence of all other celestial bodies would cause a spacecraft to deviate from its original trajectory. Therefore, the transition into the real environment is a necessary step to evaluate the feasibility of a mission. Here, the principal sources of divergence are briefly described.

Figure 3 depicts the Earth–Moon pulsation over the course of one year. The real distance of the primaries equals its mean value (384 400 km) twice every lunar orbital revolution about the Earth. Since the scaling factor adopted in the BCR4BP for the generation of the prototype trajectories is equal to the Earth–Moon mean distance, the pulsation of the system strongly affects the selection of ET_0, as will be explained later in the paper.

The orbital plane of the Moon is inclined by 5.145°with respect to the ecliptic. Equivalently, from the perspective of the Earth–Moon RPF plane, the Sun departs vertically. Figure 4 shows the solar motion over one year, approximately corresponding to the cyclic period of the pattern. This non-coplanarity introduces out-of-plane forces, and a spacecraft would deviate from its intended motion if the refinement process did not compensate for them.

3 The refinement process

This section formulates the problem of refining Earth–Moon transfers within the real dynamics. After a description of the process adopted to generate prototype trajectories in previous works, the procedure for setting optimal ET_0s is investigated. Finally, the transition to the high-fidelity model, potentially passing through the intermediate elliptic framework, is addressed.

3.1 Problem statement

3.1.1 Dataset generation

In [18] and [25], the authors generated more than 400 000 low-energy Earth–Moon trajectories in the BCR4BP, with times of flight (TOF) up to 200 days. Each bi-impulsive solution is supposed to leave the Earth

tangentially from a 167 km altitude circular Low Earth Orbit (LEO). All trajectories then insert impulsively into a 100 km altitude circular Low Lunar Orbit (LLO).

3.1.2 Clustering analysis

As a continuation of the works previously mentioned, [26] implemented an automatic dataset processing based on clustering algorithms to derive families of Earth–Moon transfers. The solutions in the dataset were initially labeled as interior, interior-exterior, and exterior based on their permanence times within the Earth–Moon region of prevalence [27]. Subsequently, clustering techniques were adopted to assess relative similarities among all solutions, thereby identifying emerging cluster families of Earth–Moon transfers. This process resulted in 23, 44, and 30 families for the interior, interior-exterior, and exterior groups, respectively. Refer to [26] for a description of the clustering procedure and results.

3.1.3 Purpose of the research

This work aims to investigate the feasibility of prototype Earth–Moon transfers in the real environment. In [26], the authors highlighted one trajectory per family based on both clustering properties and propulsive characteristics. The remainder of the paper attempts to transcribe those solutions into the real ephemeris model.

3.2 Setting the departure epoch

The choice of ET_0 is important to enable a smooth transition from prototype trajectories in the BCR4BP to the ephemeris model. The refinement process is based on the discretization of the input Earth–Moon transfer into $N-1$ evenly-spaced segments. Each discretization node n_i introduces six state variables to the refinement optimization problem, this one formulated in subsequent sections. As the initial problem is planar whereas the real system is three-dimensional, the z and z' guesses at each node are initialized to zero. To account for the transfer duration of the input trajectory in the BCR4BP, N is set equal to $\mathrm{floor}\big((\tau_\mathrm{f}-\tau_0)/0.4\big)$.

As introduced in Sect. 2.2, the scaling factor between the dynamic models matches only at specific calendar epochs. This has a strong impact when the state corresponding to the first node of a transfer, that is, the initial conditions of the prototype trajectory, is propagated in the RPRnBP. Due to the vicinity to the Earth, the dynamics is very sensitive at the departure point. Therefore, selecting ET_0 that leads to the matching of the scaling factors of the systems favors a smoother transition. Figure 5 reproduces the propagation of nodal states along a reference BCR4BP Earth–Moon transfer in the real ephemeris model at varying ET_0s (± 20 days about July 6th 2026, 1 day separation). It can be appreciated that continuity of the solution is mostly achieved when aligning the scaling factors at the instant of impulsive LEO departure, as represented by the green solution. Indeed, respecting this condition, the acceleration fields of the two dynamics are comparable. Furthermore, a similar overall scaling of the quantities is achieved, thereby obtaining transfer sections in the real environment that resemble the input counterparts. From the second node on, this effect is less pronounced and all the solutions track the same path.

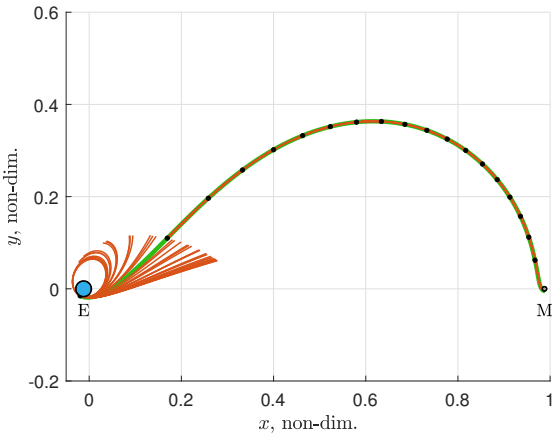

Fig. 5: RPRnBP propagation of nodal states. Green solution departs on July 6th 2026, corresponding to the green epoch highlighted in Fig. 3.

The relative angle of the Sun in the RPF is also fundamental in setting a suitable ET_0. This concept is especially important for interior-exterior and exterior transfers, where a spacecraft spends most of its TOF outside of the Earth–Moon realm and, therefore, the solar effect overcomes that of the Moon. This principle is at the base of constructing efficient exterior low-energy transfers to the Moon [12]. Since the solar attraction prevails as the spacecraft moves farther from the barycenter of the primaries, the Sun–Earth–Moon alignment should be preserved at the time of maximum distance from the RPF origin. A routine is implemented to first retrieve the Sun angle $\alpha_\mathrm{S}\big|_{\tau^*}$, where τ^* represents the time the spacecraft is the farthest during its original BCR4BP motion. Successively, a calendar year is swept to find all epochs when the same Sun–Earth–Moon alignment is achieved in the RPF, assuming planar solar motion. The dimensional TOF up to the maximum distance is subsequently subtracted from all extracted epochs, thus deriving suitable ET_0 candidates. This analysis assumes that the TOF of the refined transfer would remain equal to that of the input prototype trajectory.

The choice of a transfer ET_0 should accommodate both conditions. Approximately 27 and 12 candidate epochs over the course of one year are obtained after the pulsation and alignment analyses, respectively. The absolute differences between all epochs of the first set and those of the second set are computed. Eventually, the pair generating the minimum difference is considered, and ET_0 is set to the epoch that satisfies the pulsation condition. The process ensures a consistent representation of the trajectory at the beginning of the transfer and a proper alignment of all principal attractors at the epoch of maximum distance of the spacecraft from the Earth–Moon barycenter. In the remaining of the paper, all ET_0s belong to the 2026 calendar year and are set through the described procedure.

3.3 Ephemeris refinement process

The refinement process implemented in this work consists in formulating an optimization problem that is then solved through direct transcription and multiple shooting [28]. A first paragraph introduces the problem of discretizing input solutions, that is, the transcription part of the method. The other one formalizes the optimization problem for the direct transition into the ephemeris model.

3.3.1 Discretization of the prototype trajectory

Before proceeding with its refinement, a prototype trajectory must be sampled at some discretization nodes, as delineated at the beginning of Sect. 3.2. Nondimensional epochs when nodal BCR4BP states are extracted respect the relation

$$\tau_i = \tau_0 + \frac{i-1}{N-1}(\tau_\mathrm{f} - \tau_0) \quad \text{for} \quad i = 1, \dots, N. \tag{18}$$

To directly transition from a BCR4BP solution to its counterpart in the real ephemeris, states are provided to the optimization algorithm, this one described in the next paragraph, without further manipulations. Conversely, Sect. 3.4 exposes the procedure to be adopted when passing through the intermediate elliptic model.

3.3.2 Multiple shooting optimization

Earth–Moon transfers analyzed in this study are bi-impulsive. Therefore, besides injection points, the trajectories are ballistic and evolve only because of natural forces introduced by the environment. This formalizes the objective function of the optimization problem, that stands on minimizing the sum of departure and arrival impulsive maneuvers costs,

$$\mathcal{J} = \Delta V_\mathrm{dep} + \Delta V_\mathrm{arr}. \tag{19}$$

To calculate one contribution, for example the cost of inserting into the lunar transfer orbit, the passage through inertial dimensional quantities is necessary. Equation (15) is used to compute $\boldsymbol{R}_{\text{E-sc}}$ and $\boldsymbol{V}_{\text{E-sc}}$, vector distance of the spacecraft from the Earth and its relative velocity. Assuming the spacecraft leaves a circular Earth orbit at a certain altitude, the departure impulse expense is calculated following

$$\begin{aligned} &1) \quad \boldsymbol{h} = \boldsymbol{R}_{\text{E-sc}_1} \times \boldsymbol{V}_{\text{E-sc}_1} \\ &2) \quad \boldsymbol{s} = \boldsymbol{h} \times \boldsymbol{R}_{\text{E-sc}_1} \\ &3) \quad \Delta V_\mathrm{dep} = \left\| \boldsymbol{V}_{\text{E-sc}_1} - \sqrt{\frac{\mathrm{G}M_\mathrm{E}}{\|\boldsymbol{R}_{\text{E-sc}_1}\|}} \frac{\boldsymbol{s}}{\|\boldsymbol{s}\|} \right\|. \end{aligned} \tag{20}$$

Equivalent procedure is implemented to compute ΔV_arr at the Moon.

The optimization problem is subject to constraints to achieve transfers that comply with boundary and continuity conditions. As mentioned, the spacecraft is supposed to leave tangentially a 167 km altitude LEO, and insert into a 100 km altitude LLO. Therefore, equality constraints

$$\begin{aligned} &\|\boldsymbol{R}_{\text{E-sc}_1}\| - R_\mathrm{dep} \\ &\|\boldsymbol{R}_{\text{M-sc}_N}\| - R_\mathrm{arr} \\ &\boldsymbol{R}_{\text{E-sc}_1} \cdot \boldsymbol{V}_{\text{E-sc}_1} \\ &\boldsymbol{R}_{\text{M-sc}_N} \cdot \boldsymbol{V}_{\text{M-sc}_N} \end{aligned} \tag{21}$$

are imposed (with R representing the target dimensional distance from the body center of interest). Equations are scaled to avoid numerical issues. Ballistic continuity of the trajectory between nodal points is guaranteed by introducing additional $N-1$ equality constraints

$$\boldsymbol{\xi}_i = \boldsymbol{\varphi}([\boldsymbol{\rho}; \boldsymbol{\rho}']_i, \tau_i; \tau_{i+1}) - [\boldsymbol{\rho}; \boldsymbol{\rho}']_{i+1} \text{ for } i = 1, \dots, N-1, \tag{22}$$

where $\boldsymbol{\varphi}([\boldsymbol{\rho}; \boldsymbol{\rho}']_i, \tau_i; \tau_{i+1})$ represents the flow of the ith section of the trajectory propagated in the target RPRnBP dynamics. To conclude the formulation of the problem, inequality constraints prevent the spacecraft from impacting with either primary at the discretization points and ensure that the final time is greater than the departure epoch. Indeed, epochs $\tau_0 = \tau_1$ and $\tau_\mathrm{f} = \tau_N$ are also optimization variables, initialized to 0 and to the TOF of the input BCR4BP solution, respectively.

All transfers are refined using the MATLAB function fmincon with constraints tolerances set to 1×10^{-8}. The gradient of the objective function and the Jacobians of the constraint equations are provided analytically to the optimizer. Converging solutions are independently propagated to assess boundary conditions satisfaction and tested against impacts with either primary between nodal points. Overall, the refinement process is designed to deliver real Earth–Moon transfers that still resemble

their prototype counterparts and preserve relevant dynamical and geometrical features.

3.4 Intermediate elliptic smoothing

Direct transition to the ephemeris model may result in convergence issues due to the extreme difference in dynamic content between the BCR4BP and the RPRnBP models. An intermediate passage through the ERP favors a smoother refinement into the real dynamics. The solutions, originated in the BCR4BP, would indeed be stretched to a higher-fidelity configuration that accounts for the primaries pulsation, thereby reducing the gap between the initial and destination dynamics.

3.4.1 Elliptic model continuation

Given a departure epoch ET_0, set as per Sect. 3.2, instantaneous semi-major axis a_M, eccentricity e^*, and true anomaly f_0 of the lunar orbit about the Earth–Moon barycenter are retrieved from ephemeris data. Then, the semi-major axis of the ellipse described by the relative motion is derived as $a^* = a_\mathrm{M}/(1-\mu)$ [19]. The relative Sun angle at departure, $\alpha_\mathrm{S}\big|_{f_0}$, is corrected to reflect real ephemeris data. A continuation algorithm is implemented to gradually raise the value of the eccentricity from 0 to e^* over the course of 100 iterations. Consequently, each jth step assumes a relative semi-major axis computed as $a_j = \overline{d}(1 + e_j \cos f_0)/(1 - e_j^2)$, thus eventually converging to the target a^*.

The problem is formulated similarly to the approach in Sect. 3.3 for the ephemeris case. However, a few important differences are worth mentioning. The input prototype trajectory is sampled at intermediate non-dimensional epochs to generate the optimization variables. As the eccentricity of the first iteration, e_1, is very small, the nodal instants represent the evolution of the true anomaly of the system, which is the independent variable of the elliptic problem. The purpose of the elliptic continuation is to achieve solutions satisfying the dynamics of the ERP. Therefore, the objective function is set to one, as the minimization of the cost is to be achieved with the subsequent RPRnBP refinement. The true anomaly at departure is not an optimization variable and is fixed to f_0. Instead, f_N is still considered a degree of freedom of the problem to facilitate convergence. Each jth iteration provides the nodal inputs for the subsequent $(j+1)$th processing, until continuation achieves the target ERP.

Mixed non-dimensional/dimensional equality constraints are derived analogously to Eq. (21) as

$$\begin{aligned} &(x_1 + \mu)^2 + y_1^2 - (R_\mathrm{dep}/\ell_1)^2 \\ &(x_N + \mu - 1)^2 + y_N^2 - (R_\mathrm{arr}/\ell_N)^2 \\ &\boldsymbol{R}_{\text{E-sc}_1} \cdot \boldsymbol{V}_{\text{E-sc}_1} \\ &\boldsymbol{R}_{\text{M-sc}_N} \cdot \boldsymbol{V}_{\text{M-sc}_N}, \end{aligned} \tag{23}$$

where ℓ_i is the variable Earth–Moon distance computed at the ith node. Tangentiality constraints require transforming synodic states into primaries-centered quantities through rotation matrices. Scaling is introduced to prevent numerical issues. Finally, continuity and inequality constraints are implemented similarly to the full ephemeris direct refinement and analytical Jacobians are derived. This concludes the formulation of the elliptic continuation problem.

3.4.2 Elliptic-to-ephemeris refinement

Solutions converging to the target ERP dynamics must be manipulated before being provided to the ephemeris refinement optimizer for the final transition. An ERP solution is propagated numerically. Successively, each kth integration node is processed to change the independent variable and adjust its velocity components following

$$\begin{aligned} \boldsymbol{\rho}'_k &= \boldsymbol{x}'_k \left.\frac{\partial f}{\partial \tau_\mathrm{ell}}\right|_{f_k} \frac{\partial \tau_\mathrm{ell}}{\partial \tau_\mathrm{eph}} \\ \tau_{\mathrm{eph}_k} &= \tau_{\mathrm{ell}_k} \left(\frac{\partial \tau_\mathrm{ell}}{\partial \tau_\mathrm{eph}}\right)^{-1}, \end{aligned} \tag{24}$$

where τ_{ell_k} is retrieved from Eq. (7) and $\partial\tau_\mathrm{ell}/\partial\tau_\mathrm{eph} = \sqrt{(\overline{d}/a^*)^3}$ relates the two non-dimensional time scales. Since ephemeris refinement assumes ET_0 as guess departure epoch, τ_{eph_1} is subtracted from the temporal sequence and states are interpolated using splines. Procedure outlined in Sect. 3.3 is eventually practiced to generate nodal guesses and optimize the transfer in the real environment.

4 Earth–Moon transfers in full dynamics

Geometrically complex Earth–Moon transfers have been clustered into families in [26], thus obtaining a global portrait of possible trajectory alternatives in the planar BCR4BP. A representative solution from each family has been extracted and is refined in this work into the full ephemeris model, following the procedure described in Sect. 3.

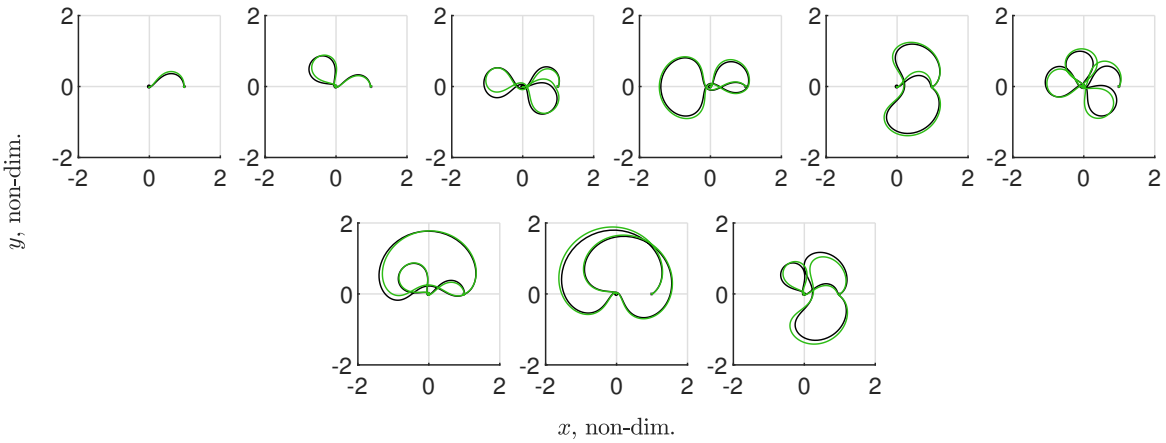

Fig. 6: Direct transition of interior BCR4BP Earth–Moon transfers (black) to their refined counterparts in the RPRnBP dynamics (green). In average, RPRnBP solutions require 10.85 m/s more than their lower-fidelity versions. Mean transfer cost is 3958.97 m/s, 32.06 days duration.

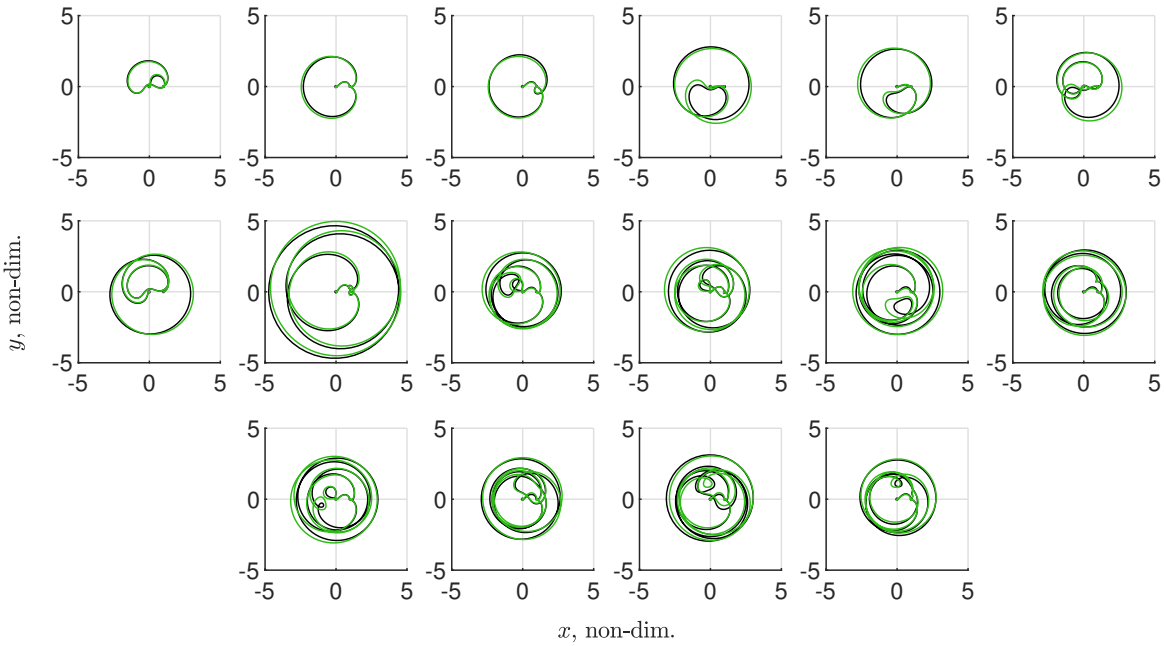

Fig. 7: Direct transition of interior-exterior BCR4BP Earth–Moon transfers (black) to their refined counterparts in the RPRnBP dynamics (green). In average, RPRnBP solutions require 6.54 m/s more than their lower-fidelity versions. Mean transfer cost is 3868.53 m/s, 121.19 days duration.

4.1 Direct ephemeris transition

4.1.1 Interior transfers

The group of interior prototype transfers comprises 23 solutions, which can be visualized in [26] for reference. Direct transition into the RPRnBP converges in only 9 cases. Variability in the number of converging solutions has been observed if changing the number of discretization points N, i.e., changing the denominator factor (default value is 0.4). Raising the number of nodes generates shorter transfer segments that generally deviate less when propagated in the full dynamics, thereby forming a larger set of input states that may facilitate the transition. However, too many sampling points may also lead to overconstraining the solution, thus preventing refinement. Solutions that could be refined by considering a certain denominator factor may not converge if a different value was assumed, and vice versa. The re-

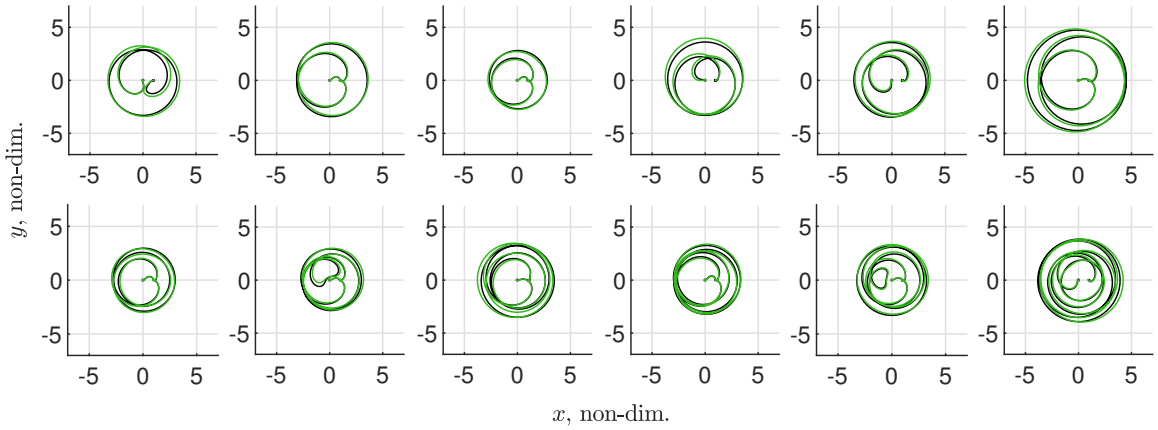

Fig. 8: Direct transition of exterior BCR4BP Earth–Moon transfers (black) to their refined counterparts in the RPRnBP dynamics (green). In average, RPRnBP solutions require 6.71 m/s more than their lower-fidelity versions. Mean transfer cost is 3837.92 m/s, 118.86 days duration.

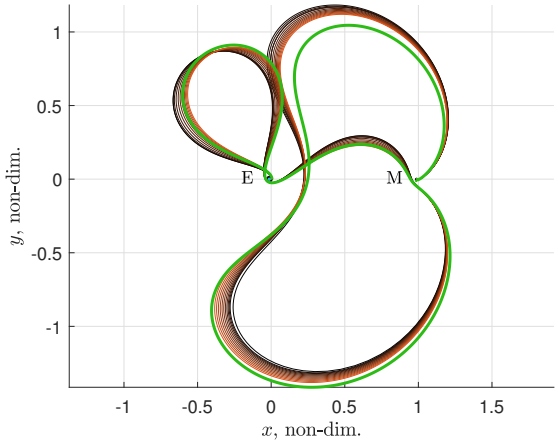

Fig. 9: Intermediate elliptic continuation, from black (BCR4BP) to orange (target ERP). Directly converging solution to the full ephemeris is represented in green. It closely follows its elliptic counterpart.

sults presented in this paper all refer to a denominator factor equal to its default value.

Figure 6 summarizes Earth–Moon transfers directly transitioning into the real environment. Solutions are represented in configuration space projected onto the planar synodic frame, as deviations in the normal direction are relatively small, and, therefore, would not be appreciable. Very complex geometries are difficult to refine because of the presence of multiple lunar flybys and/or highly-eccentric revolutions about the Earth prior to LLO insertion. That is, bi-impulsive transfers do not include mid-course maneuvers that would allow for more favorable encounters with the primary bodies during intermediate passages near them.

4.1.2 Interior-exterior transfers

Reference interior-exterior transfers are extracted from 44 cluster families and directly refined. Converging solutions are depicted in Fig. 7. The optimization algorithm converges for less than half of all the original prototype transfers, highlighting the difficulty of transitioning trajectories that exhibit very complex geometries when represented in the RPF. The challenges are similar to those of the interior case. However, completing an interior-exterior transfer requires a spacecraft to fly for a much longer TOF compared to a simple interior case. Whereas the maximum duration of an interior solution is generally less than 50 days, an exterior passage substantially increases the TOF, making convergence to the real dynamics more difficult.

4.1.3 Exterior transfers

Out of 30 reference exterior transfers, 12 solutions directly refine into the ephemeris model. Same considerations of the interior-exterior case apply in this occurrence. Figure 8 plots all exterior Earth–Moon transfers directly transitioning into the real environment. As the spacecraft leaves the Earth–Moon realm and the number of revolutions about the system in the RPF increases, the solar effect becomes increasingly predominant in guiding the motion of the spacecraft. Procedure outlined in Sect. 3.2 penalizes a correct alignment of the attractors at ET_0 to favor the correct scaling between models. This, along with the complexity of the solutions and the long transfer durations, hinders the convergence of the optimization problem.

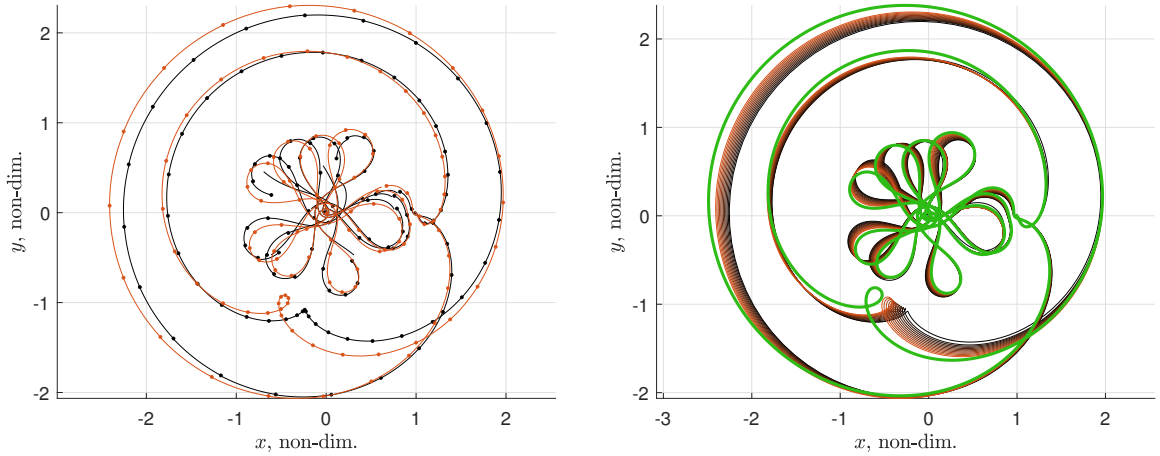

(a) Ephemeris propagation of BCR4BP (black) and ERP (orange) nodal points. Dots indicate sampling points. Elliptic solution provides a smoother and more continuous starting guess prior ephemeris optimization.

(b) Convergence to the full ephemeris solution (green) passing through the intermediate elliptic continuation (from black to orange). RPRnBP trajectory closely follows its lower-fidelity counterpart in the ERP.

Fig. 10: Example of Earth–Moon transfer requiring an intermediate elliptic continuation.

4.2 Elliptic intermediate passage

Trajectories not directly converging to the representation in the full ephemeris are subject to the intermediate elliptic smoothing described in Sect. 3.4. To prove the effectiveness of this important step, the last trajectory reported in Fig. 6 is continued into the ERP. Figure 9 depicts the continuation process, gradually adjusting the BCR4BP solution in black to match the dynamics of the target ERP, resulting in the orange trajectory. The directly refined counterpart is superimposed in green in the same figure for reference. It is evident that the optimization process, which generates the flyable trajectory, converges to a solution that shares most of its geometrical features with its lower-fidelity correspondent in the elliptic system. This confirms that the eccentricity of the Moon orbit about the Earth introduces a significant dynamic contribution that substantially alters the original motion of the spacecraft. Consequently, this intermediate step would promote a smoother convergence toward the full dynamics.

Figure 10 depicts the continuation and subsequent ephemeris refinement of a trajectory that does not permit direct transition between the extreme dynamic models. Therefore, it requires the intermediate elliptic smoothing. In particular, Fig.10a illustrates the propagation of nodal points for both the original BCR4BP (in black) and the ERP solutions (in orange) within the full dynamics. Deviations are much more prominent when propagating points belonging to the prototype trajectory, making direct refinement into the full ephemeris impossible. Conversely, in the elliptic case, an almost continuous trajectory is achieved even in proximity of sensible points such as close Earth and Moon passages, thereby providing a more accurate initial guess to the full ephemeris optimization algorithm. The green transfer in Fig. 10b represents the converged solution after optimization. The closeness to the evolution of its ERP analogue is evident.

A second refinement campaign is performed to transition the remaining Earth–Moon transfers into the ephemeris model by exploiting the intermediate passage through the ERP. Additional 4, 7, and 3 solutions for the interior, interior-exterior, and exterior groups, respectively, achieve convergence to their flyable versions and are presented in Fig. 11. Most of the refined trajectories closely follow their reference ERP solutions. However, in a few cases, the basins of attraction of the optimization algorithm result in transfers whose geometries deviate from the original shapes, as depicted in the last tile of Fig. 11. The transition into the elliptic model is deemed ineffective for exterior transfers, where the pulsation of the primaries is relevant only for very short flight periods. In all other cases, passage through the ERP is beneficial, although extremely complex geometries may still be unachievable in the real system.

5 Concluding remarks

This paper proposes a method for transitioning bi-impulse Earth–Moon transfers into the ephemeris model, which accounts for the attractive forces of principal celestial bodies and the solar radiation pressure. A dataset of thousands of solutions was processed in previous works to derive transfer families sharing common geometrical properties. In this work, one reference trajectory per family is refined into the real dynamics. Pre-

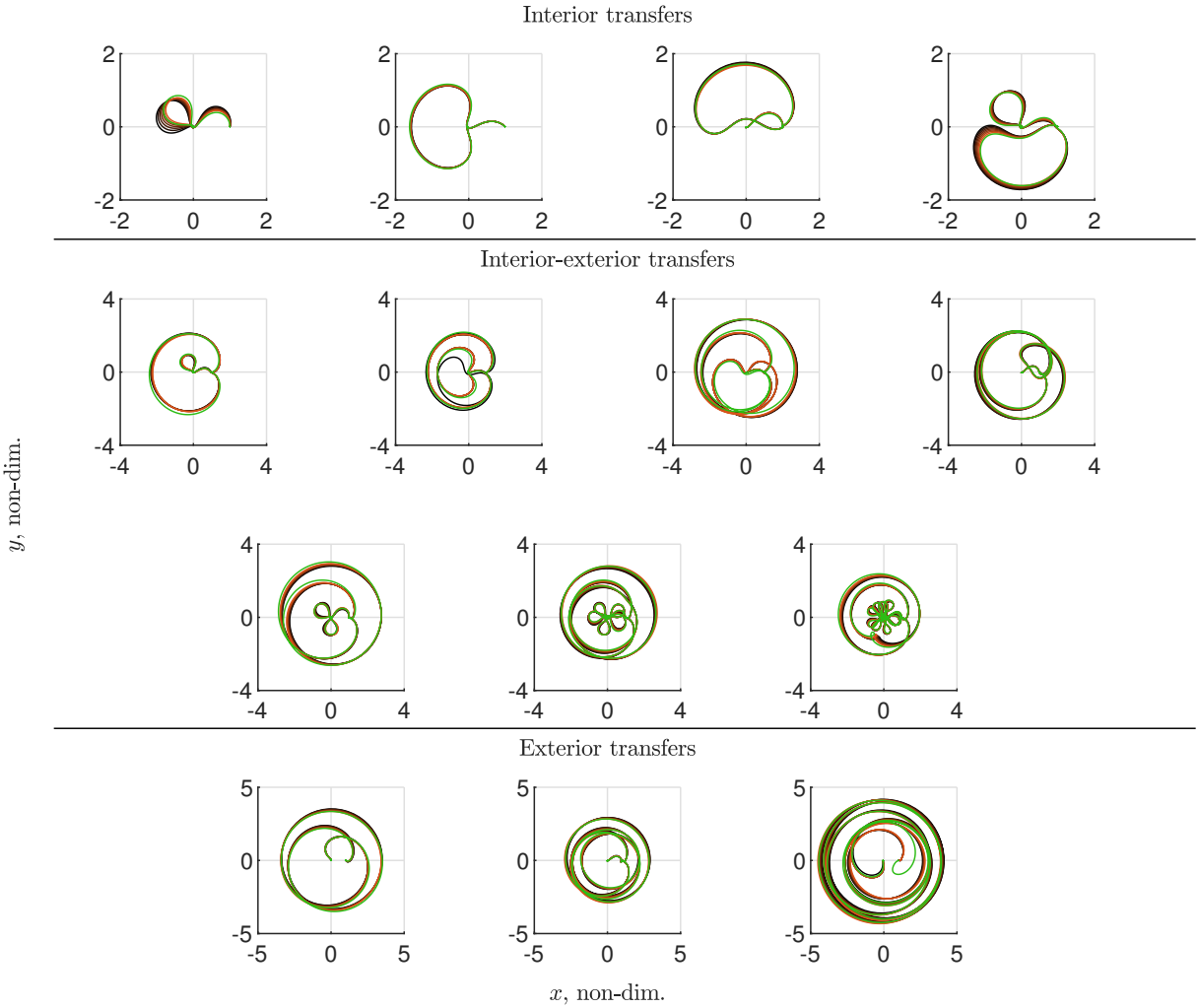

Fig. 11: Solutions converging to full dynamics (green) after elliptic intermediate transition (a few continuation steps are displayed from black to orange).

liminary design of cislunar trajectories is commonly performed in simplified models that retain only the principal dynamic contributions. However, assessing the flyability of a space trajectory in the real-world dynamics is paramount to guarantee the feasibility of the mission.

A routine to set proper calendar departure epochs is proposed. Since the full dynamics is represented in a non-dimensional roto-pulsating frame synchronized with the Earth–Moon rotation about their common barycenter, departure epochs must enable the correct matching to the reference bi-circular restricted four-body problem, which is the framework where original solutions were designed. A second constraint ensures suitable Sun–Earth–Moon relative alignments, facilitating the refinement of long-duration trajectories where the solar attraction is prominent. The beneficial effect of transitioning through the elliptic model is investigated. The pulsation of the primaries is particularly relevant for trajectories that remain within the Earth–Moon region of prevalence for long. Results demonstrate that smoother refinements toward the full ephemeris are achieved by continuing the reference trajectories into intermediate dynamic models with progressively increasing Earth–Moon eccentricity. Both elliptic and ephemeris optimization routines are formulated as nonlinear programming problems.

Convergence to the full dynamics is achieved for most of the reference trajectories. However, too complex transfer geometries are difficult to refine. Beneficial effects are obtained if transitioning through the elliptic formulation. The method is suitable for assessing the flyability of Earth–Moon transfers, thereby contributing to laying the groundwork for the next space era, where the exploitation of the cislunar environment will play a strategical role.

Bibliography

[1] M. Smith, D. Craig, N. Herrmann, E. Mahoney, J. Krezel, N. McIntyre, and K. Goodliff. The Artemis program: an overview of NASA's activities to return humans to the Moon. In *2020 IEEE Aerospace Conference*. IEEE, mar 2020.

[2] B. Cheetham. Cislunar Autonomous Positioning System Technology Operations and Navigation Experiment (CAPSTONE). In *ASCEND 2021*. American Institute of Aeronautics and Astronautics, nov 2021.

[3] V. Di Tana, B. Cotugno, S. Simonetti, G. Mascetti, E. Scorzafava, and S. Pirrotta. ArgoMoon: There is a nano-eyewitness on the SLS. *IEEE Aerospace and Electronic Systems Magazine*, 34(4):30–36, apr 2019.

[4] R. Funase et al. Mission to Earth–Moon Lagrange point by a 6U CubeSat: EQUULEUS. *IEEE Aerospace and Electronic Systems Magazine*, 35(3):30–44, mar 2020.

[5] F. Topputo et al. Meteoroids detection with the LUMIO lunar CubeSat. *Icarus*, 389:115213, jan 2023.

[6] F. Topputo, M. Vasile, and F. Bernelli-Zazzera. Low energy interplanetary transfers exploiting invariant manifolds of the restricted three-body problem. *The Journal of the Astronautical Sciences*, 53(4):353–372, dec 2005.

[7] D. A. Dei Tos and F. Topputo. On the advantages of exploiting the hierarchical structure of astrodynamical models. *Acta Astronautica*, 136:236–247, jul 2017.

[8] B. Park and K. C. Howell. Assessment of dynamical models for transitioning from the circular restricted three-body problem to an ephemeris model with applications. *Celestial Mechanics and Dynamical Astronomy*, 136(1), February 2024.

[9] M. Tan, K. Zhang, and J. Wang. Optimization of bi-impulsive Earth–Moon transfers using periodic orbits. *Astrophysics and Space Science*, 366(2), February 2021.

[10] Q. Guo and H. Lei. Families of Earth–Moon trajectories with applications to transfers towards Sun–Earth libration point orbits. *Astrophysics and Space Science*, 364(3), mar 2019.

[11] E. J. Doedel, V. A. Romanov, R. C. Paffenroth, H. B. Keller, D. J. Dichmann, J. Galán-Vioque, and A. Vanderbauwhede. Elemental periodic orbits associated with the libration points in the circular restricted 3-body problem. *International Journal of Bifurcation and Chaos*, 17(08):2625–2677, aug 2007.

[12] W. S. Koon, M. W. Lo, J. E. Marsden, and S. D. Ross. Low energy transfer to the Moon. *Celestial Mechanics and Dynamical Astronomy*, 81(1/2):63–73, 2001.

[13] J. S. Parker and R. L. Anderson. *Low-energy lunar trajectory design*. Wiley, June 2014.

[14] H. Lei, B. Xu, and Y. Sun. Earth–Moon low energy trajectory optimization in the real system. *Advances in Space Research*, 51(5):917–929, mar 2013.

[15] C. T. Campana, G. Merisio, and F. Topputo. Low-energy Earth–Moon transfers via Theory of Functional Connections and homotopy. *Celestial Mechanics and Dynamical Astronomy*, 136(3), May 2024.

[16] C. T. Campana, G. Merisio, and F. Topputo. Exterior Earth–Moon transfers design using the Theory of Functional Connections and homotopy. In *AIAA SCITECH 2024 Forum*. American Institute of Aeronautics and Astronautics, January 2024.

[17] G. Lari and C. T. Campana. The nature of the Laplace resonance between the Galilean moons, Low-energy Earth–Moon transfers via Theory of Functional Connections and homotopy. July 2024.

[18] F. Topputo. On optimal two-impulse Earth–Moon transfers in a four-body model. *Celestial Mechanics and Dynamical Astronomy*, 117(3):279–313, aug 2013.

[19] V. Szebehely and G. E. O. Giacaglia. On the elliptic restricted problem of three bodies. *The Astronomical Journal*, 69:230, apr 1964.

[20] R. S. Park, W. M. Folkner, J. G. Williams, and D. H. Boggs. The JPL planetary and punar ephemerides DE440 and DE441. *The Astronomical Journal*, 161(3):105, February 2021.

[21] C. H. Acton. Ancillary data services of NASA's Navigation and Ancillary Information Facility. *Planetary and Space Science*, 44(1):65–70, 1996. Planetary data system.

[22] C. H. Acton, N. Bachman, B. Semenov, and E. Wright. A look towards the future in the handling of space science mission geometry. *Planetary*

and Space Science, 150:9–12, 2018. Enabling Open and Interoperable Access to Planetary Science and Heliophysics Databases and Tools.

[23] D. A. Dei Tos and F. Topputo. High-fidelity trajectory optimization with application to saddle-point transfers. *Journal of Guidance, Control, and Dynamics*, 42(6):1343–1352, jun 2019.

[24] D. A. Dei Tos and F. Topputo. Trajectory refinement of three-body orbits in the real solar system model. *Advances in Space Research*, 59(8):2117–2132, apr 2017.

[25] K. Oshima, F. Topputo, and T. Yanao. Low-energy transfers to the Moon with long transfer time. *Celestial Mechanics and Dynamical Astronomy*, 131(1), January 2019.

[26] C. T. Campana and F. Topputo. Clustering of Earth–Moon transfers in Sun-perturbed environment. In *2024 IEEE Congress on Evolutionary Computation (CEC)*, volume 96, pages 1–8. IEEE, June 2024.

[27] R. Castelli. Regions of prevalence in the coupled restricted three-body problems approximation. *Communications in Nonlinear Science and Numerical Simulation*, 17(2):804–816, 2012.

[28] J. T. Betts. Survey of numerical methods for trajectory optimization. *Journal of Guidance, Control, and Dynamics*, 21(2):193–207, mar 1998.